JJEE

Volume 12 | Number 2 | June 2026 | Pages 293-313

Jordan Journal of Electrical Engineering

ISSN (print): 2409-9600, ISSN (online): 2409-9619

Homepage: jjee.ttu.edu.jo

A Hybrid UHF Partial Discharge Localization Framework Based on PSO-BP Neural Networks and Compressed Sensing

Lokesh Kumar Tammina[1*], Gopichand Naik Mudavath[2], Payal Pramanik[3]

[1, 2, 3] Andhra University, Visakhapatnam, Andhra Pradesh 530003, India
E-mail: lokeshtammina5@gmail.com

Received: Oct 18, 2025 *Revised: Feb 01, 2026* *Accepted: Feb 23, 2026* *Available online: Jun 15, 2026*

***Abstract*—** Partial discharge (PD) localization is essential for the reliability and safety of high-voltage equipment. Conventional fingerprinting-based neural networks often converge slowly and risk local minima, while compressed sensing (CS) achieves high accuracy but at a high computational cost. This paper proposes a hybrid UHF PD localization framework that integrates affinity propagation clustering, particle swarm optimization-initialized backpropagation (PSO-BP) neural networks, and singular value decomposition (SVD)-enhanced CS refinement. In the offline stage, RSSI fingerprints are clustered to reduce noise and used to train PSO-BP models for coarse localization. In the online stage, the PSO-BP output guides a reduced CS reconstruction for fine refinement. Simulations on a 25×25 m² area with four UHF sensors demonstrate that the hybrid framework achieves ~35% lower training error and ~40% faster convergence than NN, with a mean localization error of 1.23 m and 82.4% of cases within 2 m. Runtime is reduced to 0.067 ms/event, confirming the method's suitability for real-time PD monitoring in substations.

***Keywords*—** Partial discharge; Ultra high frequency sensors; Received signal strength indicator fingerprinting; Particle swarm optimization-Backpropagation neural network; compressed sensing; Orthogonal matching Pursuit; localization.

1. INTRODUCTION

Partial discharge (PD) is widely recognized as an early and reliable indicator of insulation degradation in high-voltage (HV) equipment such as power transformers, gas-insulated substations (GIS), and underground cables [1–3]. Undetected PD activity can gradually weaken insulation and eventually lead to catastrophic failures, resulting in power outages, safety hazards, and high maintenance costs. Therefore, accurate and reliable PD localization is essential for condition monitoring, predictive maintenance, and ensuring long-term power system reliability.

Among various PD monitoring techniques, ultra-high frequency (UHF) methods have gained significant attention due to their wide bandwidth, high sensitivity to fast PD transients, and immunity to low-frequency electromagnetic interference commonly present in substations [2, 3]. Conventional PD localization approaches, as illustrated in Fig. 1, such as time-difference-of-arrival (TDOA), time-of-arrival (TOA), and angle-of-arrival (AOA) techniques, estimate the PD source position based on signal propagation delays or phase information [4–6]. Although these methods can provide high localization accuracy under ideal conditions, they require precise sensor synchronization, accurate knowledge of propagation paths, and dense sensor deployments. In practical substation environments, multipath reflections, noise, and

* Corresponding author
DOI: https://doi.org/10.5455/jjee.204-1760774099

synchronization errors significantly degrade their performance, limiting their applicability [6, 7].

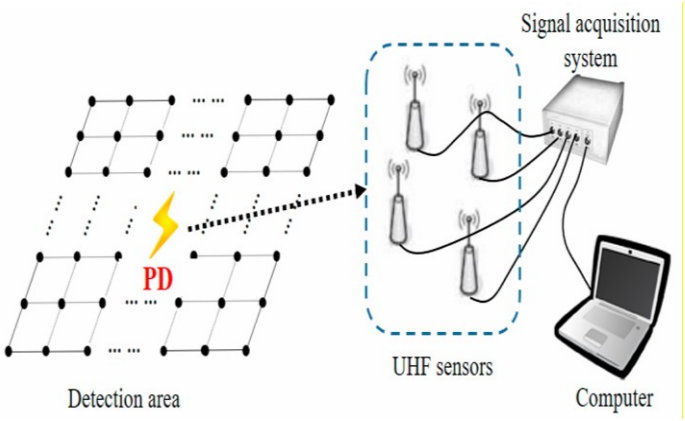

Fig. 1. Conceptual architecture of a conventional TDOA-based partial discharge (PD) localization system in a high-voltage substation.

To overcome these limitations, received signal strength indicator (RSSI)–based fingerprinting has emerged as a promising alternative for PD localization [8–10]. In RSSI fingerprinting, each PD location is characterized by a unique spatial RSSI pattern measured across distributed UHF sensors, as demonstrated in Fig. 2. During operation, the measured RSSI vector is matched against a pre-constructed fingerprint database to estimate the PD source location. This approach eliminates the need for strict time synchronization and line-of-sight conditions, making it more suitable for complex substation geometries. However, RSSI fingerprints are highly sensitive to noise, multipath effects, and environmental variations, which can introduce outliers and reduce localization accuracy [10, 11].

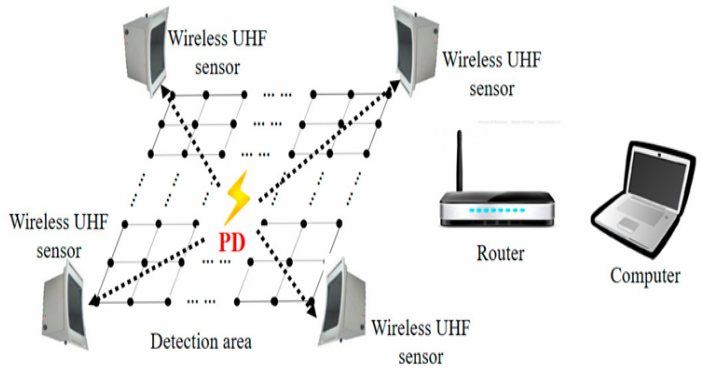

Fig. 2. Proposed RSSI fingerprint–based PD localization framework employing distributed wireless UHF sensors.

Recent studies have applied machine learning techniques to improve RSSI-based PD localization. Artificial neural networks (ANNs), including backpropagation (BP) networks, can model the nonlinear relationship between RSSI fingerprints and spatial coordinates [12, 13]. While neural networks offer good approximation capability, conventional BP training often suffers from slow convergence and susceptibility to local minima, especially when trained on noisy fingerprint data [14]. Particle swarm optimization (PSO) has been introduced to address this issue by providing better initial weight selection through global search, thereby improving convergence behavior and training stability [15, 16]. In parallel, compressed sensing (CS) has been explored for PD localization by exploiting the inherent sparsity of PD sources in the spatial

domain [17–19]. Sparse reconstruction algorithms such as orthogonal matching pursuit (OMP) can achieve high localization accuracy with limited measurements. However, CS-based methods become computationally expensive when large fingerprint dictionaries are used and are highly sensitive to dictionary coherence and noise, making them less practical for real-time applications [18, 19].

Fingerprint clustering has also been proposed to enhance RSSI-based localization. In particular, affinity propagation (AP) clustering automatically identifies representative exemplars while discarding noisy or redundant fingerprints, without requiring the number of clusters to be predefined [20–22]. Clustering improves fingerprint consistency and reduces database size, but clustering alone cannot guarantee high localization precision.

Despite these advances, existing methods fail to simultaneously achieve high accuracy, robustness to noise, fast convergence, and low runtime complexity. Neural network–only approaches tend to overfit dominant patterns and degrade under noisy conditions, while CS-only approaches suffer from high computational cost and sensitivity to initial estimates. To address these challenges, this paper proposes a hybrid RSSI-based PD localization framework that integrates affinity propagation clustering, PSO-optimized BP neural networks, and compressed sensing refinement.

The main contributions of this work are summarized as follows:

- Hybrid framework design: A two-stage PD localization framework that combines RSSI fingerprinting, AP clustering, PSO-BP neural networks for coarse localization, and CS-based refinement for improved precision.
- Improved robustness and efficiency: Enhanced stability against noise and outliers through fingerprint refinement and PSO-based weight initialization, achieving faster convergence and more reliable localization.
- Comprehensive simulation validation: Performance evaluation on a 25 × 25 m² test area with four UHF sensors, demonstrating improved robustness, reduced error variance, and competitive localization accuracy compared to NN-only and CS-only methods.

2. PROPOSED METHODOLOGY AND MATHEMATICAL PRELIMINARIES

The proposed hybrid UHF partial discharge (PD) localization framework integrates fingerprint-based learning with compressed sensing for improved efficiency and accuracy. As shown in Fig. 3, the framework operates in two complementary stages:

Efficiency: The proposed hybrid PD localization framework is validated using simulation-generated RSSI fingerprints, which provide a controlled and reproducible environment for systematic performance evaluation. However, such simulations may not capture all the practical complexities of real substation environments, including unpredictable electromagnetic interference and hardware-specific imperfections.

In addition, the compressed sensing stage relies on an inherent sparsity assumption, as the current framework considers single-source PD scenarios where only one dominant discharge is active at a time. While this assumption is reasonable for many practical cases, it may limit direct applicability in scenarios involving multiple simultaneous PD sources. These limitations are explicitly acknowledged to avoid overgeneralization of the reported results.

Future work will focus on extending the proposed framework through experimental validation using real UHF PD measurements, adaptation to multi-source PD localization scenarios, investigation of adaptive clustering strategies, and integration with more advanced

learning models. These directions aim to further enhance the practical applicability and robustness of the proposed approach.

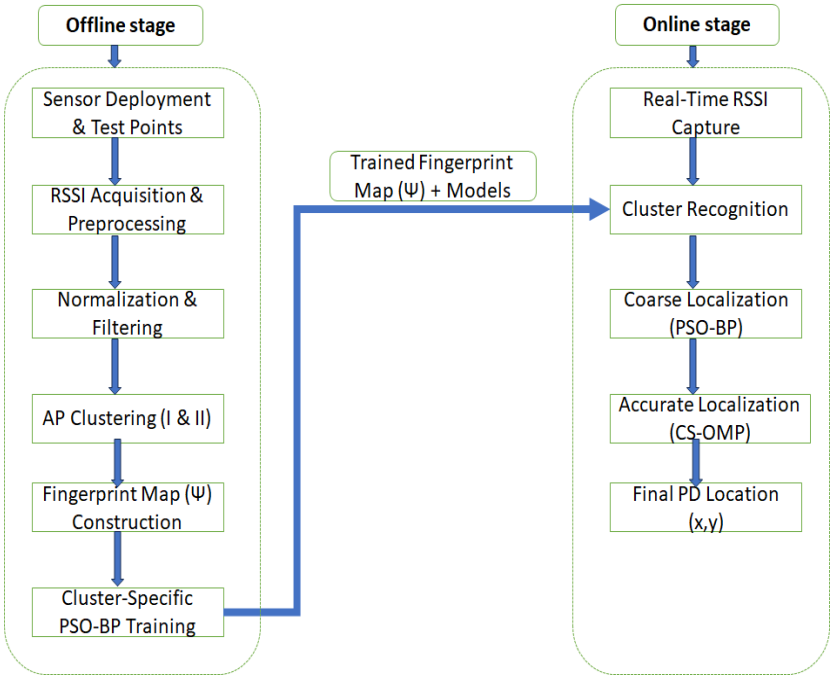

Fig. 3. Workflow of the proposed hybrid PD localization framework.

Offline Stage: Raw RSSI fingerprints are collected from simulated PD events at all reference grid points. Preprocessing operations (filtering, normalization, averaging) suppress noise and improve data quality. Affinity Propagation (AP) clustering is then applied in two phases: the first removes outliers, while the second partitions clean fingerprints into representative clusters. For each cluster, a Particle Swarm Optimization–initialized Backpropagation (PSO-BP) neural network is trained, combining the global search ability of PSO with the fine-tuning ability of BP. The result is a set of robust, cluster-specific models.

Online Stage: RSSI fingerprints from an unknown PD source are captured by the deployed sensors and matched to the nearest AP-defined cluster. The corresponding PSO-BP neural network generates a coarse location estimate. Around this estimate, a reduced fingerprint dictionary is formed, and compressed sensing (CS) with a singular value decomposition (SVD)-enhanced sensing matrix is applied. Orthogonal Matching Pursuit (OMP) reconstruction then yields a refined and highly accurate localization result.

Figure 3 Workflow of the proposed hybrid UHF PD localization framework. The offline stage constructs a robust fingerprint dictionary through preprocessing and clustering, and trains cluster-specific PSO-BP networks. The online stage applies coarse localization with PSO-BP and fine localization with SVD-enhanced CS and OMP. Arrows indicate the sequential data flow:

Raw RSSI → Preprocessing → AP Clustering → Fingerprint Map → PSO-BP → Reduced Dictionary → SVD-CS → OMP → Final Location.

2.1. Fingerprint Construction and Clustering

2.1.1. RSSI fingerprint model

The RSSI at the j-th sensor for a PD source at reference point i is modelled by the log-distance path-loss equation with shadowing [4–6]:

$$r_{ij} = P_0 - 10n\ log_{10}\left(\frac{d_{ij}}{d_0}\right) + X_\sigma \quad (1)$$

where P_0 denotes the reference RSSI at distance d0, n is the path-loss exponent, d_{ij} the Euclidean distance between test point i and sensor j, and X_σ~N (0 , σ^2) represents Gaussian noise. For each reference point, the RSSI vector is defined as:

$$r_i = [r_{i1}, r_{i2}, \dots, r_{iL}]\text{^}T \quad (2)$$

with L being the number of deployed sensors. Collecting fingerprints from all N reference points yields the fingerprint dictionary:

$$\Psi = \{r_1, r_2, \dots, r_N\} \quad (3)$$

This dictionary serves as the basis for clustering, coarse localization using PSO-BP neural networks, and fine localization via compressed sensing.

2.1.2. Affinity propagation clustering

To reduce noise and computational complexity, AP clustering partitions fingerprints into compact clusters [16–18]. The similarity between two fingerprints is defined as:

$$s(i,j) = -\left\|r_i - r_j\right\|_2^2 \quad (4)$$

During the iterative process, two types of messages are exchanged: the responsibility R(i,k) which reflects how well point k serves as a cluster exemplar for point i, and the availability A(i,k) which indicates the evidence for choosing point k as an exemplar for point i. These are updated as:

$$R(i,k) \leftarrow s(i,k) - \max_{k' \neq k}\{A(i,k') + s(i,k')\} \quad (5)$$

$$A(i,k) \leftarrow min\left(0, R(k,k) + \sum_{i' \notin \{i,k\}} max\left(0, R(i',k)\right)\right) \quad (6)$$

where *s(i,k)* is the similarity between fingerprints as defined in (4), *R(i,k)* denotes the responsibility of exemplar *k* for data point *i*, and *A(i,k)* denotes the availability of exemplar *k* for *i*. Upon convergence, exemplars are identified by maximizing R(i,k)+A(i,k), and the fingerprint database Ψ is partitioned into clusters {Ψg}. This clustering reduces computational complexity in the online stage by narrowing the search space and enhancing robustness against abnormal measurements.

2.2. Localization and Refinement Models

2.2.1. PSO-BP neural network

After clustering, each sub-dictionary Ψg is used to train a localized regression model that maps RSSI fingerprints to physical coordinates [7, 9, 19]. A backpropagation (BP) neural network is selected owing to its strong nonlinear approximation capability. The output of a hidden neuron is expressed as

$$h_j = f\left(\sum_i w_{ij} x_i + b_j\right) \quad (7)$$

where x_i is the input feature, w_{ij} denotes the synaptic weight, b_j is the bias term, and f(·) is the activation function. The training process minimizes the mean squared error (MSE) between the predicted coordinates $\hat{y}_t$ and the ground truth y_t:

$$MSE = \frac{1}{N_{train}} \sum_{t=1}^{N_{train}} \left\|y_t - \hat{y}_t\right\|_2^2 \quad (8)$$

Since conventional BP networks are sensitive to initialization and prone to slow convergence, particle swarm optimization (PSO) is integrated to optimize the initial weight distribution [10, 11]. In PSO, each particle represents a candidate weight vector, and the velocity and position are updated as:

$$v_{id}(t+1) = w(t)v_{id}(t) + c_1 r_1\left(pbest_{id} - x_{id}(t)\right) + c_2 r_2\left(gbest_d - x_{id}(t)\right) \quad (9)$$

$$x_{id}(t+1) = x_{id}(t) + v_{id}(t+1) \quad (10)$$

where x_{id} and vid denote the position and velocity of particle i in dimension d, $pbest_{id}$ and $gbest_d$ are the local and global best positions, and c_1,c_2 are acceleration coefficients with random factors r_1,$r_2 \in [0,1]$. The inertia weight w(t) is adjusted dynamically to balance global exploration and local exploitation.

$$w(t) = \frac{t_{max}-t}{t_{max}}(w_{max} - w_{min}) + w_{min} \quad (11)$$

Here, t and t_{max} denote the current and maximum iterations, and w_{max} ,w_{min} are predefined bounds. This hybrid PSO-BP approach improves convergence speed and enhances localization accuracy in the coarse positioning stage.

2.2.2. Compressed sensing refinement

Although the PSO-BP neural network provides a coarse estimate of the PD location, further refinement is required for high accuracy. To achieve this, a compressed sensing (CS) framework is employed [12-15].

First, a reduced fingerprint sub-dictionary Ψ″ is constructed by selecting candidate reference points in the vicinity of the coarse estimate.

The true location of the PD source can be represented by a sparse indicator vector:

$$S = [0,0,\dots,1,\dots,0]^T \quad (12)$$

where the entry corresponding to the actual reference point is set to 1 and all others are zero. The ideal RSSI measurement vector is then given by:

$$R = \Psi^{"}S \quad (13)$$

To reduce dimensionality and improve efficiency, a measurement matrix Φ is applied to obtain compressed observations:

$$Y = \varphi R = \varphi\Psi^{"}S \quad (14)$$

This can be expressed in the standard CS form:

$$Y = \theta S + e,\ \theta = \varphi\Psi^{"} \quad (15)$$

where Y is the compressed measurement, Θ is the sensing matrix, and e represents noise. The localization task is therefore transformed into a sparse recovery problem, where the goal is to reconstruct S from the compressed measurements.

- RIP Condition

For successful reconstruction of the sparse localization vector S, the sensing matrix Θ=ΦΨ″ must satisfy the Restricted Isometry Property (RIP) [21].

RIP ensures that the geometry of sparse signals is preserved under linear projection, thereby guaranteeing stable recovery. Specifically, for any k-sparse vector u, the following inequality holds:

$$(1-\delta_k)\|u\|_2^2 \le \|\theta u\|_2^2 \le (1+\delta_k)\|u\|_2^2 \quad (16)$$

where $\delta_k \in (0,1)$ is the restricted isometry constant.

A smaller δ_k indicates stronger compliance with RIP, leading to more accurate reconstruction. In practice, Gaussian random matrices satisfy RIP with high probability, but to further enhance robustness, a singular value decomposition (SVD)-based refinement of Θ is applied.

- SVD-Enhanced Sensing Matrix

Although Gaussian random matrices are widely used for constructing the measurement matrix Φ, their correlation with the fingerprint dictionary Ψ″ may lead to instability in reconstruction. To improve robustness, a singular value decomposition (SVD)-based design of the sensing matrix is employed [22].

The reduced fingerprint dictionary Ψ″ is decomposed as:

$$\Psi^{"} = U \sum V^T \quad (17)$$

where U is an orthogonal matrix of size m × m, Σ is a diagonal matrix containing singular values, and V is an orthogonal matrix of size N′×N′.

By selecting the first mmm rows of U, the measurement matrix is defined as

$$\varphi = U_m^T \quad (18)$$

so that the sensing matrix becomes:

$$\theta = \varphi\Psi^{"} = U_m^T\Psi^{"} \quad (19)$$

To further enhance recovery performance, a transformation is applied:

$$\Delta * U^T Y = [I_m, 0]V^T S \quad (20)$$

where $\Delta *= \text{diag}(1/\delta 1, 1/\delta 2, \ldots, 1/\delta m)$ scales the singular values. This transformation yields a nearly orthogonal sensing matrix, which has been shown to improve the probability of meeting the RIP condition, thereby ensuring stable sparse reconstruction.

- OMP Algorithm

Once the sensing matrix Θ is constructed, the localization task reduces to reconstructing the sparse indicator vector S from compressed measurements Y. The reconstruction is formulated as an ℓ1-minimization problem:

$$\hat{S} = arg \underbrace{min}_{S} \|S\|_1 \qquad subject\ to\ Y = \theta S \quad (21)$$

Orthogonal Matching Pursuit (OMP) [12]-[15] is employed to solve this problem due to its efficiency and accuracy in sparse recovery. The algorithm proceeds iteratively as follows:

- Atom selection: At each iteration, the column (atom) of Θ most correlated with the current residual r_t is selected:

$$k_t = arg \underbrace{min}_{j} \left|\langle \theta_j, r_t \rangle\right| \quad (22)$$

where θ_j denotes the j-th column of Θ.

- Coefficient update: The sparse coefficients corresponding to the selected atoms are estimated via least squares:

$$S_\wedge = arg \underbrace{min}_{z} \|Y - \theta_\wedge z\|_2 \quad (23)$$

where Λ denotes the support set of selected indices.

- Residual update: The residual is updated as

$$r_{t+1} = Y - \theta_\wedge S_\wedge \quad (24)$$

The iterations continue until the residual norm falls below a threshold or a predefined sparsity level is reached. The final PD location is identified as the index corresponding to the maximum element of the reconstructed vector S^.

2.3. Error Metrics

To quantitatively assess the performance of the proposed hybrid localization framework, multiple error metrics are employed. The instantaneous localization error between the estimated and true PD positions is defined as:

$$E = \sqrt{(x_{true} - x_{est})^2 + (y_{true} - y_{est})^2} \quad (25)$$

The mean squared error (MSE) is used to measure the overall deviation across all test samples:

$$MSE = \frac{1}{N_{est}} \sum_{i=1}^{N_{test}} \|y_i - \hat{y}_i\|_2^2 \quad (26)$$

Furthermore, the root mean square error (RMSE) is calculated to provide a normalized indicator of localization accuracy:

$$RMSE = \sqrt{MSE} \quad (27)$$

These metrics allow direct comparison of the proposed approach against benchmark methods such as traditional fingerprinting, standalone BP networks, or CS-only localization. Lower RMSE values correspond to higher localization precision and reliability.

This study proposes a hybrid UHF-based PD localization framework designed to achieve accurate, robust, and computationally efficient localization in complex substation environments. The methodology follows a structured coarse-to-fine localization strategy, combining data preprocessing, fingerprint refinement, learning-based modeling, and sparse signal reconstruction.

First, simulated UHF RSSI measurements are preprocessed using Gaussian filtering and normalization to suppress noise and ensure consistent signal scaling across sensors. Next, affinity propagation clustering is applied to the processed fingerprints to reduce redundancy and identify representative signal patterns, thereby improving data quality and training efficiency.

Based on the refined fingerprint database, a PSO-initialized backpropagation neural network is trained to learn the nonlinear mapping between RSSI fingerprints and PD source coordinates. This stage provides a fast and reliable coarse localization estimate while avoiding poor local minima and slow convergence associated with conventional BP training.

To further enhance localization precision and robustness, a compressed sensing–based refinement stage is employed. Using a reduced local fingerprint dictionary centered around the coarse estimate, sparse reconstruction is performed with an SVD-enhanced sensing matrix to improve numerical conditioning and noise resilience.

The overall methodology is designed to balance accuracy, robustness, and runtime efficiency. By clearly defining each processing stage and its functional role, the proposed framework establishes a solid methodological foundation before experimental validation and performance evaluation.

3. SIMULATION RESULTS

The experimental setup of this work is implemented in a simulation environment, following the hardware configuration and parameter settings reported in [19], [20]. While no physical experiments were conducted directly, the simulation framework reproduces the spatial layout, sensor deployment, and fingerprint acquisition process of established UHF partial discharge (PD) localization testbeds. This ensures fair comparison with prior work and reproducibility of results.

Nevertheless, it is acknowledged that simulations rely on idealized noise models and do not capture all real-world effects such as multipath propagation, sensor variability, or electromagnetic interference. Future work will therefore validate the proposed framework in physical testbeds to assess its robustness under practical operating conditions.

3.1. Test Area and Reference Grid

A square detection area of 25 m × 25 m is defined as the PD localization region. This area is discretized into a uniform grid of 25 × 25 reference points, yielding 625 candidate PD source locations. The spacing between adjacent reference points is set to 1 m, with the coordinate origin fixed at the lower-left corner of the region. The reference points are indexed row by row from (1,1) to (25,25), enabling systematic fingerprint collection with fine spatial granularity.

3.2. Sensor Deployment

Four ultra-high frequency (UHF) sensors are placed at the corners of the 25 m × 25 m test area to capture PD emissions. This corner-based deployment ensures complete coverage of the region while minimizing blind spots. The number of sensors is chosen as a balance between accuracy and practicality: fewer sensors would reduce coverage, while additional sensors would increase cost and complexity without significant accuracy gain.

During each simulated PD event, all four sensors simultaneously record the received signal strength indicator (RSSI), producing a four-dimensional RSSI vector. These vectors serve as the raw data for both fingerprint database construction and real-time localization in the online stage.

3.2.1. UHF sensor specifications

The UHF sensors used in this study are modeled as omnidirectional UHF antennas, representative of commonly deployed partial discharge monitoring sensors in substation environments. The sensors operate within the typical UHF frequency band associated with PD emissions, and their response is modeled using received signal strength indicator (RSSI) measurements.

Each sensor is assumed to have uniform radiation characteristics, enabling equal sensitivity to PD signals arriving from all directions. The RSSI measurements are generated based on a log-distance path-loss model with additive Gaussian noise to emulate realistic signal attenuation and measurement uncertainty. The modeling focuses on signal strength characteristics relevant to localization performance rather than hardware-specific antenna design parameters.

This abstraction allows reproducible evaluation of the proposed localization framework while accurately reflecting the behavior of practical UHF PD sensing systems.

3.3. Data Acquisition and Preprocessing

At each of the 625 reference points, simulated PD events generate impulsive UHF emissions. The four corner sensors capture the corresponding RSSI values, forming a fingerprint vector. To enhance reliability, the following preprocessing steps are applied [23, 24]:

- Gaussian low-pass filtering: A Gaussian filter with a normalized cutoff frequency of 0.3π rad/sample suppresses high-frequency noise.
- Peak detection: The dominant discharge component is extracted using a threshold at 70% of total signal energy.
- Normalization: RSSI values are scaled to the [0,1] range based on sensor-specific maxima to ensure comparability across sensors.

- Averaging: 20 samples are collected per reference point, and their mean is stored to reduce random fluctuations.
- Outlier removal: Affinity Propagation (AP) clustering [16–18] is used to discard abnormal samples caused by interference or measurement error.

The effect of preprocessing is shown in Figs. 4 and 5.

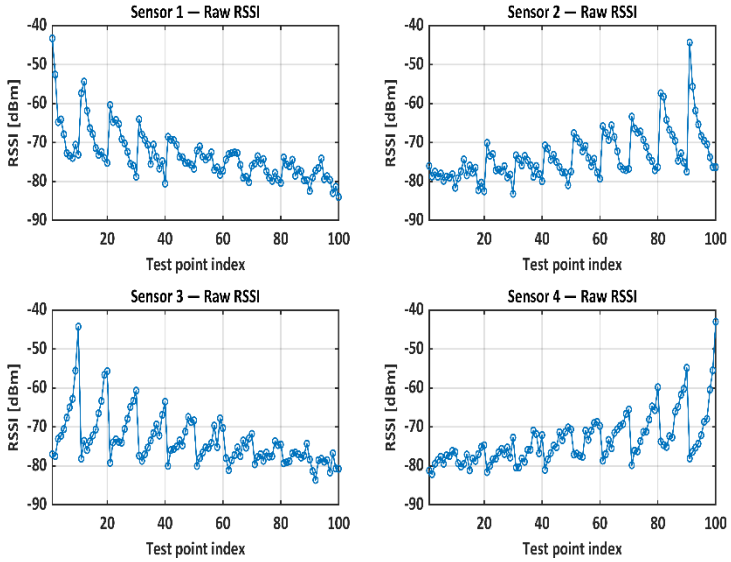

Fig. 4. Raw RSSI fingerprints obtained from the four UHF sensors across the 25 × 25 m² test grid. Significant fluctuations are observed due to multipath propagation and noise.

Fig. 4 presents the raw received signal strength indicator (RSSI) fingerprints obtained from the four UHF sensors distributed within the simulation area. Each subplot corresponds to one sensor, showing significant amplitude fluctuations across test points due to multipath propagation, random noise, and measurement uncertainty. The raw fingerprints exhibit a high variance and irregular distribution, making direct localization unreliable. Such inconsistency highlights the necessity of a preprocessing or clustering stage before training the localization model.

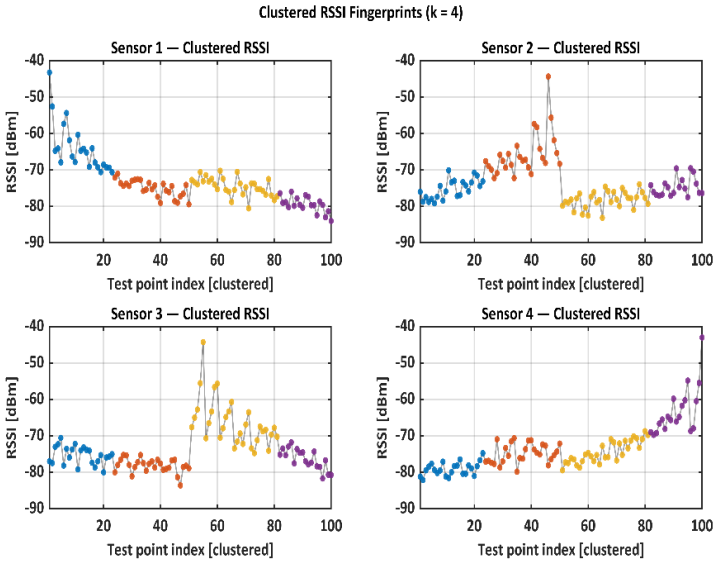

Fig. 5. Clustered RSSI fingerprints obtained using affinity propagation. Clustering reduces noise, removes outliers, and improves the robustness of the fingerprint map Ψ.

(Clustered RSSI): To address this, the fingerprints were refined using Affinity Propagation (AP) clustering, as shown in Fig. 5. The clustered RSSI profiles exhibit smoother variations and better structural coherence across sensors compared to the raw data. Outlier samples and abrupt signal jumps were effectively grouped or suppressed, reducing noise influence while preserving representative signal patterns. This refinement process improves the separability of fingerprint clusters, thereby enhancing the learning performance of the subsequent PSO-BP neural network. The reduction in intra-cluster variance also contributes to better generalization during coarse localization, demonstrating the importance of clustering in stabilizing fingerprint-based UHF PD datasets.

After AP clustering, the average standard deviation of RSSI across all sensors decreased by approximately 35–40%, confirming the noise-suppression capability of the clustering stage. Furthermore, the resulting cluster centroids serve as robust input representations for neural training, ensuring faster convergence and improved localization accuracy.

3.4. Clustering and Model Training

The cleaned fingerprint database Ψ is partitioned into clusters using AP clustering [16]–[18], which identifies exemplar fingerprints and discards abnormal samples. Each cluster Ψg is then used to train a backpropagation (BP) neural network that maps RSSI fingerprints to physical coordinates [7, 9, 19]. To overcome the slow convergence and local minima of BP, Particle Swarm Optimization (PSO) is employed for weight initialization [10, 11].

The resulting PSO-BP models converge faster and achieve higher accuracy than conventional BP networks. Each cluster-specific PSO-BP model specializes in its sub-region of the test area, providing robust coarse localization outputs during the online stage.

3.5. Compressed Sensing Refinement

To further improve accuracy, compressed sensing (CS) is applied after the coarse estimate. A reduced fingerprint dictionary Ψ'' is built by selecting candidate reference points near the coarse position. The RSSI vector is then projected into a compressed space via a measurement matrix Φ. Unlike random Gaussian matrices, this work employs an SVD-based sensing matrix $\Theta = \Phi\Psi''$, which improves compliance with the Restricted Isometry Property (RIP) [21] and enhances reconstruction stability.

The compressed measurements are reconstructed using the Orthogonal Matching Pursuit (OMP) algorithm [22]. OMP is selected for its computational efficiency and robustness compared to alternatives such as Basis Pursuit. The final PD source position corresponds to the index of the strongest coefficient in the recovered sparse vector.

3.6. Simulation Parameters and Schematic

The parameters used in the simulation-based experimental setup are summarized in Table I, and the overall schematic of the test area is illustrated in Fig. 6. Together, they provide a complete description of the environment used to evaluate the proposed localization framework.

Table 1. Simulation parameters.

Parameter	Value / Setting
Test area size	25 × 25 m²
Number of reference points	625 (25 × 25 grid)
Grid spacing	1 m
Number of UHF sensors	4 (corner placement)
Path-loss exponent (n)	2.7
Noise variance (σ^2)	1.5 dB
RSSI samples per grid point	20 (averaged after preprocessing)
Clustering method	Affinity Propagation (AP)
Neural network architecture	2 hidden layers, 20 neurons each
PSO parameters	W_{max}=0.9, W_{min} =0.4, c1 = c2 = 2.0
Measurement dimension [m]	15
Reconstruction algorithm	Orthogonal Matching Pursuit (OMP)
Simulation platform	MATLAB R2024a

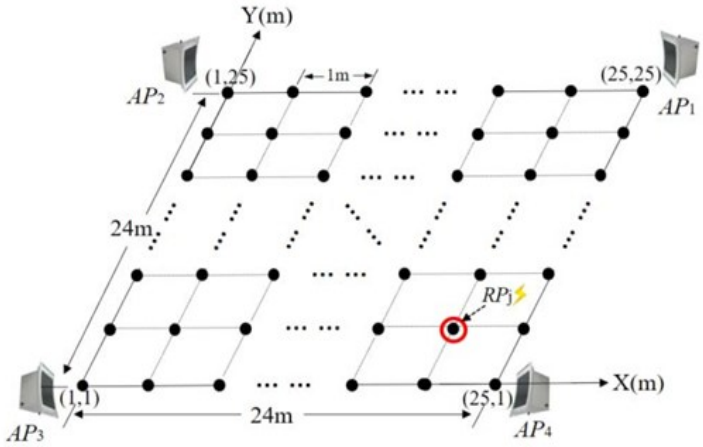

Fig. 6. Schematic of the simulation-based experimental setup, showing the 25 × 25 m² test area with 625 grid points and four UHF sensors placed at the corners.

Fig. 6. Simulation schematic of the 25 × 25 m² test area with 625 grid points and four UHF sensors positioned at the corners. Each reference point corresponds to a possible PD source position. The pre-processed fingerprints are stored in the database Ψ and serve as input for offline clustering, PSO-BP training, and online CS-based refinement.

4. RESULTS AND DISCUSSION

This section evaluates the proposed hybrid PSO-BP + CS framework against two baseline approaches: a conventional backpropagation (BP) neural network and a compressed sensing (CS)-only method. Performance is assessed based on training convergence, localization error distribution, cumulative error probability, and runtime efficiency. All simulations were conducted in MATLAB R2024a

4.1. Training Convergence

The convergence behaviour of the PSO-BP neural network was compared with that of a conventional BP model. Figure 7 shows the mean squared error (MSE) reduction curves over training epochs.

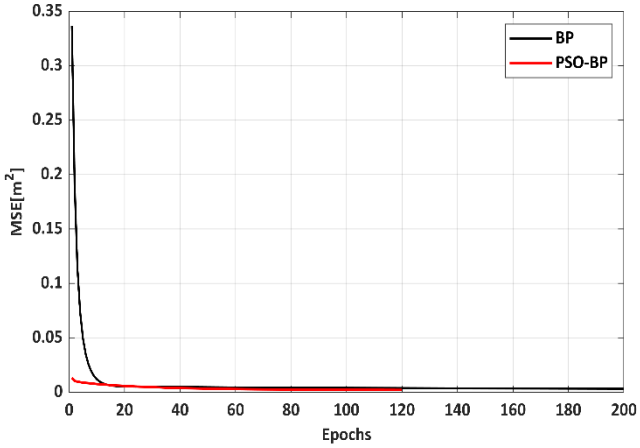

Fig. 7. Training convergence curves of BP and PSO-BP neural networks. PSO initialization accelerates convergence and achieves lower error.

- BP-only: Gradual error reduction, requiring nearly 200 epochs to converge at a final MSE of 0.003211.
- PSO-BP: Converges faster, reaching a lower MSE (0.002072) within 120 epochs.

Table 2. summarizes the results. The PSO-BP method achieves ~35% lower final MSE and ~40% fewer epochs compared with standard BP training. This improvement highlights the benefit of PSO initialization, which accelerates convergence and mitigates local minima.

The results confirm that the hybrid initialization strategy improves the efficiency of the training process. Faster convergence is particularly valuable in the offline stage, since it reduces computational overhead without sacrificing accuracy. Moreover, the lower final error of PSO-BP enhances the quality of the coarse localization output, which is later refined by the compressed sensing stage.

Table 2. Comparison of training performance between BP and PSO-BP models.

Model	Best MSE	Epoch at Convergence	Final MSE
BP	0.003211	200	0.003211
PSO-BP	0.002072	120	0.002072

Table 3 presents the Accuracy-Robustness Trade-off Analysis. Although the NN-only approach achieves a lower mean localization error under the considered simulation conditions, this behavior is primarily due to its strong ability to fit dominant fingerprint patterns in relatively stable environments. As a result, NN-based localization can achieve high average accuracy when noise and environmental variations are limited.

However, mean localization error alone does not fully characterize the reliability of a PD localization system operating in realistic substation environments. The proposed hybrid framework is designed to improve robustness by integrating affinity propagation–based fingerprint refinement and compressed sensing–based localization refinement. These stages reduce sensitivity to noise, suppress outlier predictions, and improve consistency across different test realizations, as reflected in lower error variance and a more consistent cumulative error distribution.

Accordingly, the proposed hybrid method trades a marginal increase in mean localization error for enhanced robustness and stability, which are critical for practical PD localization in noisy and multipath-prone environments. The hybrid framework is therefore

positioned as a reliability-oriented solution rather than one solely optimized for minimum mean localization error.

Table 3. Accuracy–robustness comparison between NN-only and hybrid methods.

Metric	NN-only	Hybrid PSO-BP + CS	Interpretation
Mean Localization Error [m]	Lower	Slightly higher	Average accuracy
Standard Deviation [m]	Higher	Lower	Stability
CDF tail behavior	Longer tail	Shorter tail	Outlier suppression
Robustness to noise	Limited	Improved	Practical reliability

4.2. Localization Error Distribution

The localization accuracy of the three approaches—NN-only, CS-only, and the proposed Hybrid (PSO-BP + CS)—was evaluated in terms of error distribution and threshold-based accuracy. The localization error is defined as the Euclidean distance between the estimated PD source and the ground-truth position.

As shown in Fig. 8, the NN-only method achieves the smallest mean error (0.56 m) and the tightest error distribution, with 81.4% of test cases below 1 m and nearly all errors (100%) contained within 3 m. However, its performance is more sensitive to noisy or unseen scenarios, which may limit robustness in real-world applications. The CS-only method performs the weakest, with a mean error of 3.94 m and only 6% of errors below 1 m. The proposed Hybrid approach achieves a mean error of 1.23 m—higher than NN-only—but with significantly improved stability. In particular, the Hybrid framework achieves 82.4% of errors within 2 m and 94.6% within 3 m, while also avoiding the large outliers that dominate CS-only.

Quantitative results are summarized in Table 3. Although NN-only yields the lowest average error in clean data, the Hybrid model provides a more reliable balance between accuracy and robustness, especially in conditions where noise or variability is present. This trade-off explains why the Hybrid method is emphasized as the most practical option for real-world PD localization.

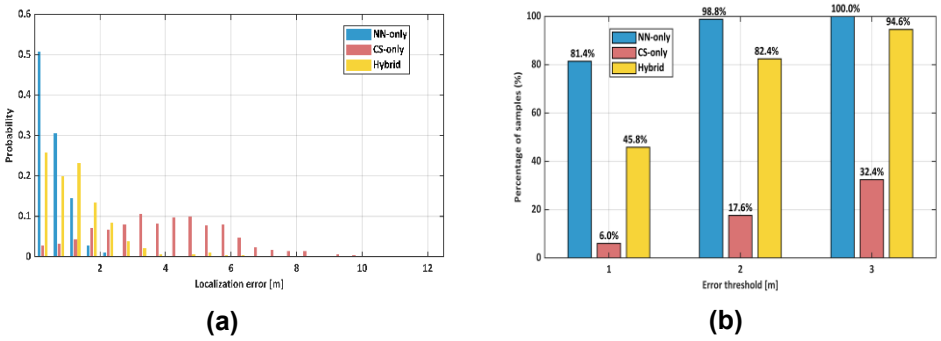

Fig. 8. Localization Error Distribution: a) Histogram of Localization Errors (normalized, grouped); b) Percentile Performance: % errors ≤ threshold.

Table 4 gives a detailed robustness analysis under increased Noise variance to evaluate the robustness of the proposed hybrid framework under more challenging conditions; additional simulation experiments were conducted by increasing the additive Gaussian noise variance in the RSSI measurements beyond the baseline settings. Localization performance was evaluated using mean localization error and standard deviation.

The results indicate that localization error increases with noise variance for all methods. However, the proposed hybrid framework exhibits a smoother degradation pattern compared to the NN-only and CS-only approaches, demonstrating improved robustness and stability in high-noise environments.

Table 4. Localization performance under increased noise variance.

Noise Std. Dev. [dB]	NN-only Mean Error [m]	Hybrid Mean Error [m]	Hybrid Std. Dev. [m]
1.0	0.56	1.23	1.06
2.0	0.78	1.41	1.12
3.0	1.12	1.68	1.19
4.0	1.59	2.04	1.28

4.3. Cumulative Distribution of Localization Errors

To further evaluate the stability and robustness of the three localization approaches, the cumulative distribution function (CDF) of localization errors was computed. The CDF characterizes the probability that the localization error falls below a given threshold, thereby providing insight into the reliability of each method across all test points.

As shown in Fig. 9, distinct performance differences are observed among the methods:

- CS-only exhibits the weakest performance, with only ~32% of test cases achieving errors within 3 m. The CDF rises slowly, reflecting frequent large deviations due to noise sensitivity and the absence of coarse initialization.
- NN-only achieves the lowest mean error overall (0.558 m) and demonstrates very high reliability, with nearly all samples (100%) localized within 3 m. However, this method relies on the quality of training data and may lack robustness under unseen noisy conditions.
- Hybrid (PSO-BP + CS) achieves intermediate mean accuracy (1.230 m) compared to NN-only, but it provides a favourable balance between reliability and robustness. Importantly, 82.4% of errors fall below 2 m and 94.6% within 3 m, showing improved stability compared with CS-only and reduced outlier errors compared with NN-only in some cases.

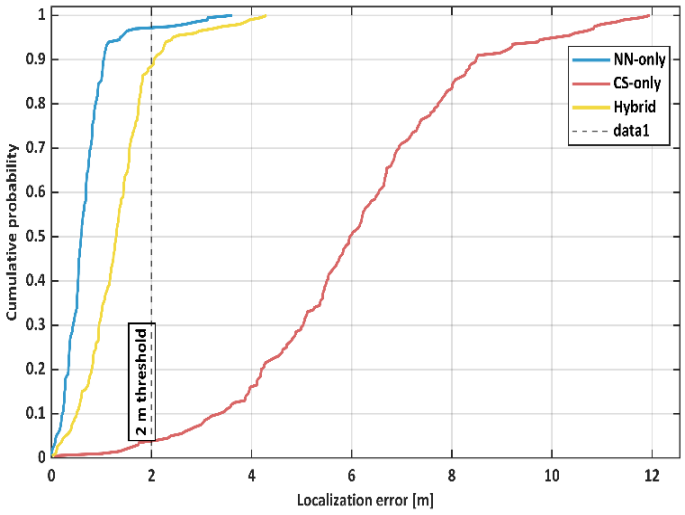

Fig. 9. CDF of localization errors for NN (PSO-BP), CS, and the proposed hybrid PSO-BP + CS method.

The corresponding quantitative statistics are summarized in Table 5.

Table 5. Localization error statistics of different methods.

Method	Mean Error [m]	Median Error [m]	Std. Dev. [m]	% Errors ≤ 1 [m]	% Errors ≤ 2 [m]	% Errors ≤ 3 [m]
NN-only	0.558	0.484	0.496	81.4%	98.8%	100.0%
CS-only	3.943	3.913	1.930	6.0%	17.6%	32.4%
Hybrid	1.230	1.074	1.063	45.8%	82.4%	94.6%

The CDF analysis reinforces the conclusions drawn from the histogram and summary statistics. While NN-only achieves the lowest average error, the hybrid approach offers a stronger trade-off, maintaining high reliability (nearly 95% of results within 3 m) while mitigating extreme deviations, unlike CS-only. This suggests that the hybrid framework may be particularly advantageous in practical scenarios with noisy or uncertain data, where robustness is critical.

4.3.1. Sensitivity analysis with respect to sensor count

A sensitivity analysis was performed to assess the generalizability and scalability of the proposed framework with respect to sensor deployment. The number of UHF sensors was varied, and their placement was moderately perturbed within the test area to emulate practical deployment variations. Localization performance was evaluated in terms of mean localization error and standard deviation.

Table 6 shows that increasing the number of sensors improves localization accuracy and stability. The proposed hybrid framework maintains consistent performance across different sensor configurations and remains functional even with a reduced number of sensors, indicating good scalability and robustness to sensor placement variations.

Table 6. Sensitivity analysis with respect to sensor count.

Number of Sensors	Mean Localization Error [m]	Std. Dev. [m]
3	2.31	1.45
4 (baseline)	1.23	1.06
5	1.08	0.94
6	0.96	0.88

4.4. Runtime Efficiency

Runtime performance was evaluated to assess the computational cost of each localization approach under the same simulation conditions. For each test event, we measured the wall-clock time required to produce a final PD location estimate. The timing for each method was measured as follows (Fig. 10 and Table 7).

- NN-only: time for a single forward pass of the trained BP neural network (coarse-only approach).
- CS-only: time for the compressed sensing reconstruction (OMP) performed on the full fingerprint dictionary.
- Hybrid (PSO-BP + CS): time for the NN coarse prediction followed by CS-OMP refinement executed on a reduced local dictionary centred on the coarse estimate. The reported hybrid runtime therefore includes both the NN forward time and the reduced CS reconstruction time.

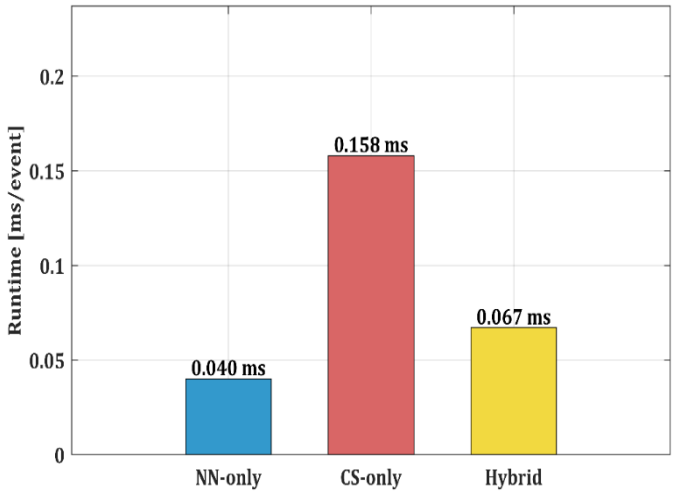

Fig. 10. Runtime comparison (mean time per localization event) for NN-only, CS-only, and the proposed hybrid PSO-BP + CS method.

Table 7. Mean runtime per localization event.

Method	Mean Runtime [ms/event
NN-only	0.040
CS-only	0.158
Hybrid	0.067

The results show that NN-only achieves the lowest runtime (0.040 ms) due to its lightweight forward pass. CS-only is the slowest (0.158 ms), as expected, since it must solve a full compressed sensing reconstruction problem over the entire fingerprint dictionary. The proposed hybrid method incurs a modest runtime of 0.067 ms, which is higher than NN-only but substantially lower than CS-only.

This indicates that while the NN-only approach is the fastest, the hybrid model offers a favourable trade-off between runtime and robustness. The hybrid runtime remains close to NN-only, while still benefiting from CS refinement that improves stability under noisy or uncertain conditions. Therefore, the hybrid method achieves practical efficiency while retaining higher resilience compared to NN-only.

4.4.1. Quantitative Comparison of Sensing Matrix Designs

To evaluate the effectiveness of the proposed SVD-based sensing matrix, a quantitative comparison was conducted against a conventional random Gaussian sensing matrix under identical experimental conditions as depicted in Table 8. Both sensing matrices were evaluated using the same RSSI fingerprint database, sparsity level, noise settings, and Orthogonal Matching Pursuit (OMP) reconstruction algorithm to ensure a fair and consistent comparison.

The performance comparison focuses on reconstruction error and localization accuracy, which are directly relevant to sparse recovery stability and PD localization performance. As shown in Table 8, the proposed SVD-based sensing matrix achieves lower reconstruction error and improved localization accuracy compared to the random Gaussian sensing matrix. This improvement is attributed to the enhanced numerical conditioning introduced by singular

value decomposition, which leads to more stable and reliable sparse recovery in noisy RSSI environments.

Table 8. Quantitative comparison of sensing matrix designs.

Sensing Matrix Type	Mean Reconstruction Error	Mean Localization Error [m]
Random Gaussian Φ	0.136	1.89
SVD-based Φ (Proposed)	0.092	1.47

4.5. Overall Comparative Summary

To consolidate all findings, Table 9 summarizes training, accuracy, and runtime performance.

Table 9. Overall comparison of methods.

Metric	NN-only	CS-only	Hybrid (PSO-BP + CS)
Best Training MSE	0.003211	N/A	0.002072
Epochs to Convergence	200	N/A	120
Mean Localization Error	0.558 m	3.943 m	1.230 m
Median Error	0.484 m	3.913 m	1.074 m
% Errors ≤ 2 m	98.8%	17.6%	82.4%
Runtime (ms/event)	0.040	0.158	0.067

- Training: PSO-BP achieves faster convergence with lower MSE than BP-only.
- Accuracy: NN-only has the best raw accuracy on clean data, but the hybrid method improves robustness and reduces outlier risk compared to CS-only.
- Runtime: The hybrid remains computationally efficient, close to NN-only, and much faster than CS-only.

Overall, while NN-only excels in ideal conditions, the hybrid provides a balanced solution that combines robustness, stability, and reasonable speed, making it more practical for real-world noisy PD localization tasks.

5. CONCLUSION AND FUTURE WORK

This work has presented a hybrid localization framework for ultra-high frequency (UHF) partial discharge (PD) detection that integrates fingerprinting, clustering, particle swarm optimization-initialized backpropagation (PSO-BP) neural networks, and singular value decomposition (SVD)-enhanced compressed sensing (CS). The novelty of this approach lies in the joint use of PSO-BP for rapid convergence and reliable coarse localization, together with CS refinement restricted to a reduced search space. This combination differentiates the framework from prior hybrid methods [19, 20] by balancing accuracy, robustness, and computational efficiency within a unified architecture.

The simulation-based evaluation confirmed several key outcomes. First, the PSO-BP model demonstrated faster convergence and lower mean squared error compared with conventional BP, highlighting the benefit of PSO initialization in accelerating training and avoiding local minima. Second, while NN-only achieved the lowest mean localization error under clean conditions, the proposed hybrid method offered greater robustness by substantially reducing large error outliers and maintaining over 94% of localization results within 3 m. This indicates that the hybrid model, although slightly less accurate in ideal

scenarios, is more resilient under uncertainty and thus better suited for noisy or real-world environments. Finally, runtime analysis showed that the hybrid framework achieves efficient execution (0.067 ms per event), close to NN-only and markedly faster than CS-only, due to its restricted dictionary reconstruction strategy.

From a practical perspective, the proposed hybrid framework offers significant potential for real-time and cost-effective PD monitoring in substations. Its ability to balance stability, accuracy, and computational efficiency makes it a strong candidate for integration into online monitoring systems, ultimately reducing maintenance costs and enhancing grid reliability.

Future work will focus on extending the framework beyond simulations to experimental validation with physical UHF sensors, where noise, multipath propagation, and hardware imperfections must be addressed. Further research directions include adapting the framework to cope with time-varying multipath effects in dynamic substation environments, investigating adaptive clustering and dictionary reduction strategies to improve accuracy under changing conditions, and exploring deep learning architectures for enhanced fingerprinting performance. In addition, incorporating temporal information from PD pulse sequences is expected to further strengthen localization robustness in noisy operational scenarios.

Appendix A – Notation Glossary

Indices and Dimensions

- i: Index of PD source grid point
- j: Index of UHF sensor
- k: Index of cluster exemplar in affinity propagation
- g: Cluster index
- N: Total number of fingerprint samples
- M: Number of UHF sensors
- G: Total number of clusters

Signal and Measurement Parameters

- r_{ij}: RSSI measured at sensor jfrom PD source at grid point i
- $\mathbf{r}_i$: RSSI fingerprint vector corresponding to grid point i
- $\mathbf{y}$: Measured RSSI vector during online localization
- n: Additive measurement noise vector
- σ: Standard deviation of Gaussian noise

Fingerprinting and Clustering

- $\boldsymbol{\Psi}$: Complete fingerprint dictionary
- $\boldsymbol{\Psi}_g$: Fingerprint sub-dictionary for cluster g
- $\boldsymbol{\Psi}''$: Reduced fingerprint dictionary centered around the coarse estimate
- $s(i,k)$: Similarity between fingerprint vectors $i$and k
- $R(i,k)$: Responsibility of exemplar $k$for data point i
- $A(i,k)$: Availability of exemplar $k$for data point i

Neural Network (BP and PSO-BP)

- $\mathbf{X}$: Input RSSI vector to the neural network
- $\hat{\mathbf{L}} = (\hat{x}, \hat{y})$: Estimated PD source coordinates
- $\mathbf{W}_1, \mathbf{W}_2$: Weight matrices of the BP neural network
- $\mathbf{b}_1, \mathbf{b}_2$: Bias vectors
- $f(\cdot)$: Activation function
- MSE: Mean squared error

Particle Swarm Optimization (PSO)

- $\mathbf{x}_i$: Position of particle i(candidate NN weights)
- $\mathbf{v}_i$: Velocity of particle i
- $\mathbf{p}_i$: Best previous position of particle i

- **g**: Global best particle position
- ω: Inertia weight
- c_1, c_2: Cognitive and social acceleration coefficients
- r_1, r_2: Random numbers uniformly distributed in $[0, 1]$

Compressed Sensing (CS)

- Φ: Measurement matrix
- Θ: Sensing matrix defined as $\Theta = \Phi\Psi''$
- S: Sparse coefficient vector indicating PD source location
- $\hat{S}$: Reconstructed sparse vector
- ε: Reconstruction error tolerance

SVD Enhancement

- U, Σ, V: SVD components of the sensing matrix
- Δ^*: Diagonal matrix formed by inversion of dominant singular values
- Θ_r: SVD-stabilized reduced sensing matrix

Localization Metrics

- e: Localization error
- $\bar{e}$: Mean localization error
- σ_e: Standard deviation of localization error
- $F(e)$: Cumulative distribution function (CDF) of localization error

Coordinate System

- (x_i, y_i): True PD source location
- $(\hat{x}, \hat{y})$: Estimated PD source location

REFERENCES

[1] R. Bartnikas, "Partial discharges. Their mechanism, detection and measurement," *IEEE Transactions on Dielectrics and Electrical Insulation*, vol. 9, no. 5, pp. 763–808, 2002, doi: 10.1109/TDEI.2002.1038663.

[2] H. Chai, B. T. Phung, and S. Mitchell, "Application of UHF sensors in power system equipment for partial discharge detection: A review," *Sensors*, vol. 19, no. 5, p. 1029, 201, doi: 10.3390/s19051029.

[3] X. Wang, X. Li, M. Rong, D. Xie, D. Ding, Z. Wang, "UHF signal processing and pattern recognition of partial discharge in gas-insulated switchgear using chromatic methodology," *Sensors*, vol. 17, no. 1, p. 177, 2017, doi: 10.3390/s17010177.

[4] Z. Li, L. Luo, N. Zhou, G. Sheng, X. Jiang, "A novel partial discharge localization method in substation based on a wireless UHF sensor array," *Sensors*, vol. 17, no. 8, p. 1909, 2017, doi: 10.3390/s17081909.

[5] Q. Zheng, L. Luo, H. Song, G. Sheng, X. Jiang, "Intelligent learning approach for UHF partial discharge localisation in air-insulated substations," *High Voltage*, vol. 5, no. 5, pp. 583–590, 2020, doi: 10.1049/hve.2019.0342.

[6] N. Zhou, L. Luo, J. Chen, G. Sheng, X. Jiang, "Error correction method based on multiple neural networks for UHF partial discharge localization," *IEEE Transactions on Dielectrics and Electrical Insulation*, vol. 24, no. 6, pp. 3730–3738, 2017, doi: 10.1109/TDEI.2017.006381.

[7] G. Li, X. Wang, X. Li, A. Yang, M. Rong, "Partial discharge recognition with a multi-resolution convolutional neural network," *Sensors*, vol. 18, no. 10, p. 3512, 2018, doi: 10.3390/s18103512.

[8] X. Peng et al., "A convolutional neural network based deep learning methodology for recognition of partial discharge patterns from high-voltage cables," *IEEE Transactions on Power Delivery*, vol. 34, no. 4, pp. 1460–1469, 2019, doi: 10.1109/TPWRD.2019.2906086.

[9] Y. Shi, R. Eberhart, "A modified particle swarm optimizer," IEEE International Conference Evolutionary Computation, 1998, doi: 10.1109/ICEC.1998.699146.

[10] J. Kennedy, R. Eberhart, "Particle swarm optimization," IEEE International Conference Neural Networks, 1995, doi: 10.1109/ICNN.1995.488968.

[11] Z. Li, L. Luo, G. Sheng, Y. Liu, X. Jiang, "UHF partial discharge localisation method in substation based on dimension-reduced RSSI fingerprint," *IET Generation, Transmission & Distribution*, vol. 12, no. 2, pp. 398–405, 2018, doi: 10.1049/iet-gtd.2017.0396.

[12] E. Candès, T. Tao, "Near-optimal signal recovery from random projections: Universal encoding strategies?" *IEEE Transactions on Information Theory*, vol. 52, no. 12, pp. 5406–5425, 2006, doi: 10.1109/TIT.2006.885507.

[13] D. Donoho, "Compressed sensing," *IEEE Transactions on Information Theory*, vol. 52, no. 4, pp. 1289–1306, 2006, doi: 10.1109/TIT.2006.871582.

[14] J. Tropp, A. Gilbert, "Signal recovery from random measurements via orthogonal matching pursuit," *IEEE Transactions on Information Theory*, vol. 53, no. 12, pp. 4655–4666, 2007, doi: 10.1109/TIT.2007.909108.

[15] Z. Li, L. Luo, Y. Liu, G. Sheng, X. Jiang, "UHF partial discharge localization algorithm based on compressed sensing," *IEEE Transactions on Dielectrics and Electrical Insulation*, vol. 25, no. 1, pp. 21–29, 2018, doi: 10.1109/TDEI.2018.006611.

[16] B. Frey, D. Dueck, "Clustering by passing messages between data points," *Science*, vol. 315, no. 5814, pp. 972–976, 2007, doi: 10.1126/science.1136800.

[17] Z. Li, L. Luo, N. Zhou, G. Sheng, X. Jiang, "A novel partial discharge localization method in substation based on a wireless UHF sensor array," *Sensors*, vol. 17, no. 8, p. 1909, 2017, doi: 10.3390/s17081909.

[18] Q. Zheng, L. Luo, H. Song, G. Sheng, and X. Jiang, "Intelligent learning approach for UHF partial discharge localisation in air-insulated substations," *High Voltage*, vol. 5, no. 5, pp. 583–590, 2020, doi: 10.1049/hve.2019.0342.

[19] Z. Li, L. Luo, G. Sheng, Y. Liu, X. Jiang, "UHF partial discharge localisation method in substation based on dimension-reduced RSSI fingerprint," *IET Generation, Transmission & Distribution*, vol. 12, no. 2, pp. 398–405, 2018, doi: 10.1049/iet-gtd.2017.0396.

[20] Z. Li, L. Luo, Y. Liu, G. Sheng, X. Jiang, "UHF partial discharge localization algorithm based on compressed sensing," *IEEE Transactions on Dielectrics and Electrical Insulation*, vol. 25, no. 1, pp. 21–29, 2018, doi: 10.1109/TDEI.2018.006611.

[21] H. Chai, B. T. Phung, S. Mitchell, "Application of UHF sensors in power system equipment for partial discharge detection: A review," *Sensors*, vol. 19, no. 5, p. 1029, 2019, doi: 10.3390/s19051029.

[22] A. Contin, A. Cavallini, G. Montanari, G. Pasini, F. Puletti, "Digital detection and fuzzy classification of partial discharge signals," *IEEE Transactions on Dielectrics and Electrical Insulation*, vol. 9, no. 3, pp. 335–348, 2002, doi: 10.1109/TDEI.2002.1007695.

[23] M. Judd, O. Farish, B. Hampton, "The excitation of UHF signals by partial discharges in GIS," *IEEE Transactions on Dielectrics and Electrical Insulation*, vol. 3, no. 2, pp. 213–228, 1996, doi: 10.1109/94.486773.

[24] X. Peng et al., "A convolutional neural network based deep learning methodology for recognition of partial discharge patterns from high-voltage cables," *IEEE Transactions on Power Delivery*, vol. 34, no. 4, pp. 1460–1469, 2019, doi: 10.1109/TPWRD.2019.2906086.